Proceedings World Geothermal Congress 2010
Bali, Indonesia, 25-29 April 2010

Analysis of Well Tests in Afyon Ömer-Gecek Geothermal Field, Turkey

Mustafa Onur

Department of Petroleum and Natural Gas Engineering, Istanbul Tech. U., Maslak, 34469, Istanbul, Turkey

onur@itu.edu.tr

Keywords: Well Testing, Afyon Ömer-Gecek, Analysis, pressure-derivative, deconvolution

ABSTRACT

In this work, analyses of pressure transient tests (such as multirate tests, conventional drawdown/buildup tests, and interference tests) conducted in the Afyon Ömer-Gecek geothermal field, Turkey, are presented. The pressure transient tests were conducted at six different wells. The pressure data were acquired by downhole quartz gauges, and thus, amenable to the applications of modern well-test analysis techniques such as derivative and deconvolution. Deconvolution analysis based on recently proposed robust algorithms was found useful to extract more information from the variable-rate well tests conducted in the field. In general, the pressure data analyzed indicate that the wells' productivities are quite high, but influenced by non-Darcy flow effects and are producing in a complex fractured/faulted network system. The estimated values of permeability-thickness products (kh) from buildup and interference tests range from 40 to 1900 darcy-m, whereas porosity-compressibility-thickness products ($\phi c_t h$) estimated from the interference tests range from 2.91×10^{-4} to 1.06×10^{-2} psi/m.

1. INTRODUCTION

Located in the central Aegean region of Turkey and 15 km northeast of the city of Afyon (Figure 1), the Ömer-Gecek geothermal field is one of the important geothermal fields in Turkey.

The geothermal system can be classified as a low-temperature, single-phase liquid-dominated one containing geothermal water (having salinity of 4 000 to 6 000 ppm and dissolved CO_2 content about 0.4% by weight) with temperatures ranging from 50 to 111.6°C. The wells (nearly 30) drilled in the field range in depth from 56.8 to 902 m. The total production rate from the field is about 236 kg/s and the geothermal water produced has been utilized to support a district heating system with a capacity of approximately 4500 residences and some health spa facilities since 1996 (Satman *et al*., 2007).

The Ömer-Gecek geothermal system is a convective hydrothermal type commonly occur in areas of active geological faulting and folding, and areas where the regional heat flow is above normal, as in much of the western Turkey. As for the geology of the system, mica schist and marbles of Paleozoic age forms the basement of the field. At the same time, these rocks form the reservoir system. Neogene deposits composed of conglomerate, sandstone, clayey limestone-sandstone, and volcanic glass-trachandesitic tuff unconformably overlie the Paleozoic basement. Satman *et al.*, (2007) provides further details about the geology, well depths, well temperatures, geochemical analysis of the geothermal water.

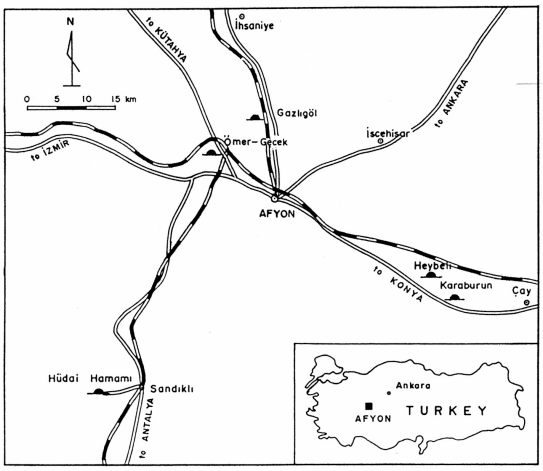

Figure 1. Location map of the Ömer-Gecek geothermal field.

Although the field was explored in 1960s, not much quantitative information on reservoir characteristics (permeability, fault/fracture networks, wells' IPRs etc.), which is essential for understanding and modeling the production performance of the wells and the field, was available. To acquire such information, pressure transient tests were designed and conducted in the field in 2004. Well tests were conducted at six wells; AF-10, AF-11, AF-16, AF-20, AF-21, and R-260. Further information regarding these wells (location, depth, temperature of the geothermal fluid produced, etc) are given by Satman *et al.* (2007).

The objective of this work was to determine wells' productivities, estimation of permeability-thickness and porosity-compressibility-thickness products, as well as to determine reservoir characteristics (single layer, multi-layer, double porosity, etc.) and reservoir boundaries (faults and their flow characteristics) by the analyses of pressure transient tests conducted in the field.

2. MULTIRATE TESTS

Here, we summarize the results obtained from the analyses of multirate tests conducted at the wells AF-11, AF-16, AF-20, and AF-21. Multirate tests are designed to construct the inflow performance relationship (IPR) of those wells as well as to determine reservoir parameters and characteristics from the pressure signal recorded by using conventional as well as modern well-test analyses techniques based on recently proposed deconvolution algorithms by von Schroeter *et al.* (2004) and Levitan (2005). Only pressure/rate data for the multirate test of the well AF-21 and its analysis will be presented here.

The multirate test of AF-21 consists of a well-test sequence (four distinct step rate changes and one shut-in period) acquired over a 16-hour test. Figure 2 presents the pressure and rate data for this well-test sequence (note that a single pressure buildup profile of about 4 hr is acquired at the end of the testing sequence).

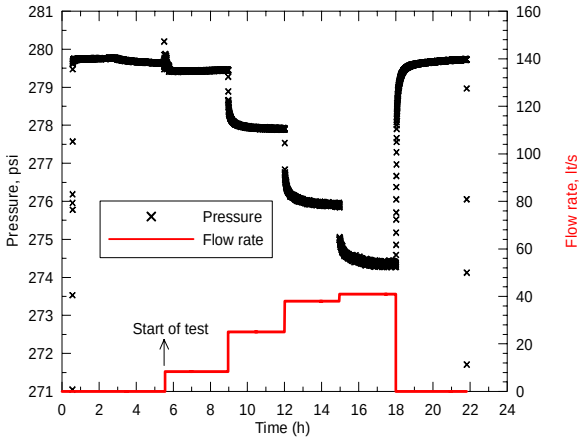

Figure 2. Pressure and rate data for the multirate test conducted at the well AF-21.

The pressure measurements shown in Fig. 2 were taken from a down-hole quartz gauge set a depth of 195 m (total depth of the well is 210 m), and rate measurements were taken at the surface using a weir. In this example, the measured initial pressure is approximately 280.0 psi, but there is some uncertainty in this value. The maximum pressure measured in the test sequence was 279.872 psi. The temperatures recorded at 195 m was nearly constant at 107.8 ^{o}C.

Figure 3 shows the IPR curve obtained from the multirate test conducted at the well AF-21. The IPR curve fitted through measured pressure drop data is described best by the steady-state "turbulent" flow model (Eq. 1). The second term bq^2 in the right-hand side of equation is due to non-Darcy flow. The non-Darcy effect observed on the IPR curve of the well AF-21 (as well as on those of other wells tested) is possibly due to a high permeability fracture network system intersecting the well. Because of this, flow rate near the wellbore is so high that the flow regime becomes "turbulent" in the vicinity of the wellbore. Thus Darcy's law loses its validity, and hence the bq^2 term in the right-hand side of Eq. 1 becomes important to well deliverability.

$$\Delta p = aq + bq^2, \qquad (1)$$

The estimated values of the parameters a and b in Eq. 1 from the multirate test for the well AF-21 and multirate tests conducted for the wells AF-11, AF-20, and AF-21 are given in Table 1. IPR curves constructed for these wells are compared in Figure 4. From Figure 4, it can be seen that IPR curves for all four wells tested indicate a non-Darcy flow model represented Eq. 1 and that the well AF-21 is the most productive amongst four wells.

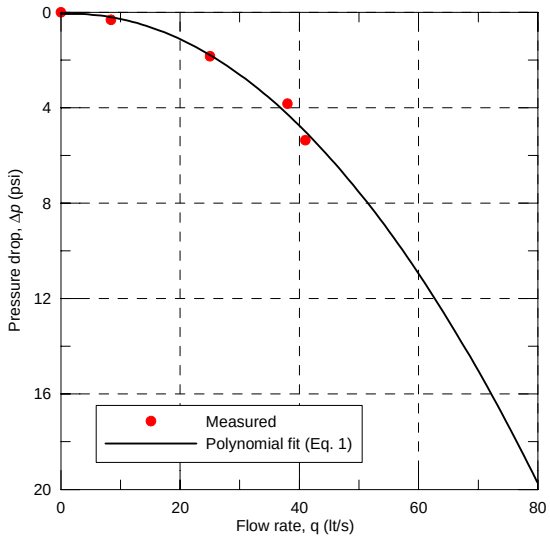

Figure 3. IPR curve for well AF-21, obtained from multirate test data shown in Fig. 2.

Table 1. Parameters of IPR curves for Wells AF-11, AF-16, AF-20, and AF-21, determined from multirate tests.

Well Name	a psi/(lt/s)	b psi/(lt/s)^2	p_i (psi) @ depth (m)
AF-11	0.0985	0.00418	147.9 @ 107 m
AF-16	0.0408	0.00276	236.4 @ 174 m
AF-20	0.0249	0.00265	131.8 @ 98 m
AF-21	0.0120	0.00321	279.8 @ 195 m

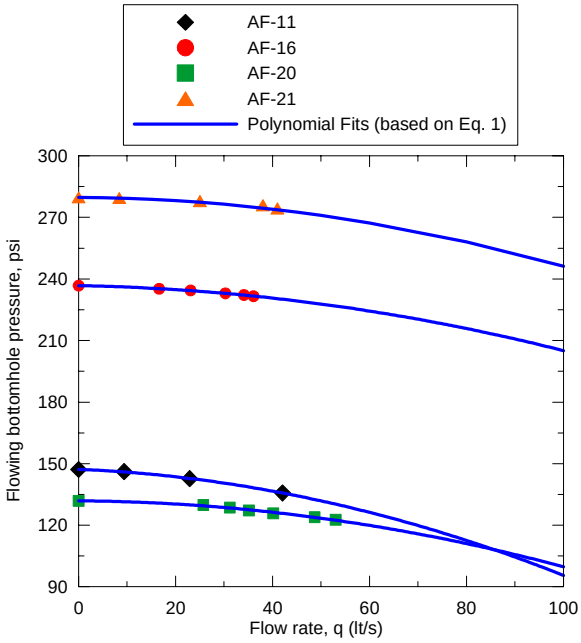

Figure 4. IPR curves for the wells AF-11, 16, 20 and 21, constructed from multirate tests.

Although IPR curves and IPR parameters such as *a* and *b* are useful for understanding the deliverability of wells, and for tubular design purposes, unfortunately, the reservoir parameters such as permeability-thickness product and skin as well as information about reservoir characteristics and boundaries cannot be derived from the "lumped" parameters *a* and *b* of IPR curves. To estimate such parameters and information, one must analyze the pressure signal, particularly, recorded during the buildup period of multirate tests.

Therefore, next, we analyzed the pressure signal recorded during the multirate tests. Here, we will present a detailed analysis only for the multirate test of the well AF-21. Figure 5 shows log-log plots of conventional rate normalized multirate pressure change vs. elapsed time for each flow period. This graph shows clearly that pressure change data for each flow period are more or less displaced by a constant value. Moreover, as the flow rate increases, the displacement becomes larger. This is possibly due to rate-dependent skin due to non-Darcy flow. Although not shown here, we have also looked at the Bourdet derivatives (Bourdet *et al.*, 1989) for each flow period, these derivative signals indicate changing (and/different) wellbore storage effects (possibly due to non-isothermal/multiphase flow inside the wellbore) at early times of each flow period.

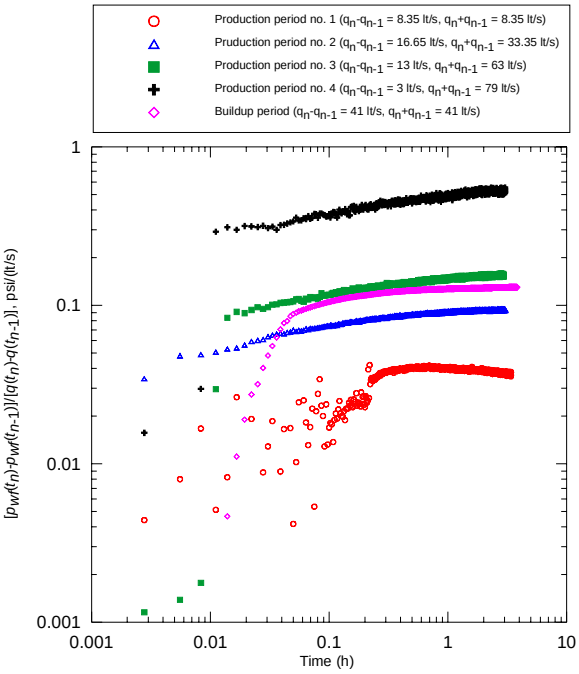

Figure 5. Log-log plot of normalized pressure changes vs. elapsed time for each flow period of the multirate test of the well AF-21.

To eliminate the multirate effects and convert the multirate data into an equivalent unit-rate constant drawdown response, we applied a robust deconvolution algorithm developed by Onur *et al.* (2008) by accounting for all flow rate history (Fig. 2). As is known (Bourdet, 2002), conventional drawdown or buildup analysis based on superposition-time transform does not completely remove all effects of previous rate variations and often complicates test analysis due to residual superposition effects.

It is worth noting that the Onur *et al.* deconvolution algorithm used here is based on the ideas presented by von Schroeter *et al.* (2004) and Levitan (2005), and is based on minimization of a weighted least-squares (LS) objective function given by

$$O(z_1,z_2,...,z_N,q_1^u,q_2^u,...,q_{N_r}^u,p_0)=\frac{1}{2}\sum_{i=1}^{N_p}\left[\frac{p_0-p_{m,i}-\Delta p_{model}(t_i)}{\sigma_{p,i}}\right]^2 + \frac{1}{2}\sum_{j=1}^{N_r}\left[\frac{q_{m,j}-q_j^u}{\sigma_{q,j}}\right]^2 + \frac{1}{2}\sum_{k=1}^{N-1}\left[\frac{\kappa_{c,k}}{\sigma_{c,k}}\right]^2 \qquad (2)$$

Here, *O* represents the weighted LS objective function as a function of unknown parameters listed in the left-hand side of Eq. 2. Note that the model parameters are the response function z , the rate q , and the initial pressure p_0 . Here z is equal to the natural logarithm (or the Bourdet derivative) of unit-rate drawdown response, that is, $z = \ln[dp_u(t)/d\ln t]$ (where $p_u(t)$ represents drawdown pressure drop if the well were produced at constant unit-rate; see Onur *et al.*, 2008). The rate q plays dual role. q can be treated as one of model parameters. q is also the part of the data that must be fitted to the model.

In Eq. 2, N represents the total number of nodes at which the z-responses are to be computed, N_p represents the total number of measured pressure points to be history matched, and N_r is the total number of measured (or allocated) flow rate steps to be treated as unknown in history matching process. It is worth noting that the objective function considered is quite general because it allows one to perform simultaneous estimation of z responses at each node and the initial reservoir pressure p_0, as well as any flow rate steps in the rate sequence. In all applications given in this paper, we use $N = 70$.

In Eq. 2, $\sigma_{p,i}$ represents the standard deviation of error in measured pressure $p_{m,i}$ at time t_i. Typically, in applications, we can assume identically distributed normal errors with zero mean and the same specified standard deviation for each measured pressure point; that is, $\sigma_{p,i}=\sigma_p;\quad for\quad i=1,2,\cdots,N_p$. Similarly, $\sigma_{q,j}$ represents the standard deviation of error in measured (or allocated) rate step $q_{m,j}$ to be treated as unknown. $\sigma_{c,k}$ represents the "standard deviation" of the curvature constraint $\kappa_{c,k}$. As suggested by von Schroeter *et al.* (2004) and Levitan (2005), we set $\sigma_{c,k}=\sigma_c$ for all k, equal to one constant value. We have found that $\sigma_c = 0.05$ often works well. This value has been chosen to provide small degree of regularization and at the same time not to over constrain the problem and create significant bias. Selection of the parameters σ_c, σ_p, and σ_q usually depends on the quality of the data available and may require a trail-and-error procedure and the subjective judgment of the interpreter [see Onur *et al.* (2008) for further details].

We processed the pressures for the entire test sequence in one pass to estimate the initial pressure and rates jointly with the unit-rate derivative response functions. The deconvolved constant rate responses are compared with the conventional buildup responses in Figure 6. All responses

are based on the last flow rate prior to buildup, which is equal to 41 lt/s. The initial pressure estimated from deconvolution is equal to 280.081, compared to the maximal pressure in the test sequence of 279.872 psi which was used as an initial guess for the initial reservoir pressure.

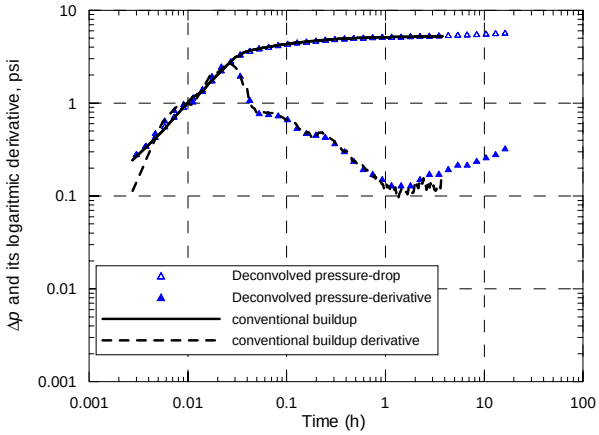

Figure 6. Comparison of deconvolved responses with the conventional pressure buildup pressure change and its Bourdet derivative (normalized by the last rate prior to buildup) for the well AF-21.

As we do not have prior knowledge of the error level in rate data; it is difficult for us to judge whether the rate estimated from deconvolution (shown in Fig. 7) (with an average *rms* error of 4.95 lt/s) is acceptable: The rates for the first two flow periods are changed by approximately 30%, which is quite large, while the rates for the third and fourth flow periods are changed by approximately 11%.

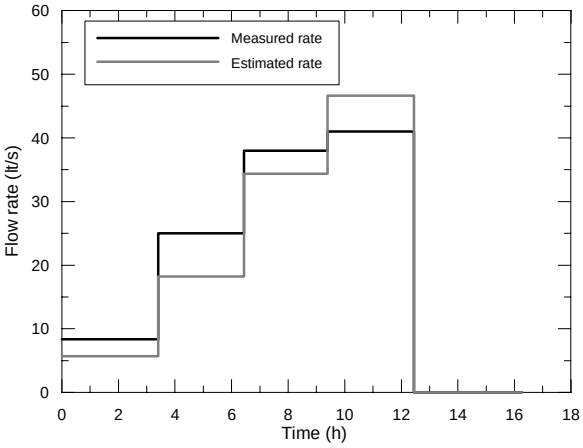

Figure 7. Comparison of measured and estimated rate by deconvolution for the well AF-21.

The prior geologic model (Fig. 8) indicates that the well is located near the faults, but no information exists whether the faults are no-flow or conductive. The deconvolved unit-rate response indicates that these faults may be no-flow because of a well-defined 1/2 slope line after one hour (Fig. 7). The deconvolved derivative response at early-times from 0.003 to 0.2 hr gives an indication of a partially or fully penetrating well with changing wellbore-storage effect. In addition, the -1 slope line in the time interval from 0.3 to 1 hr exhibited by the deconvolved derivative response may indicate that the well is near a highly conductive fault or permeability-thickness product increasing away from the well.

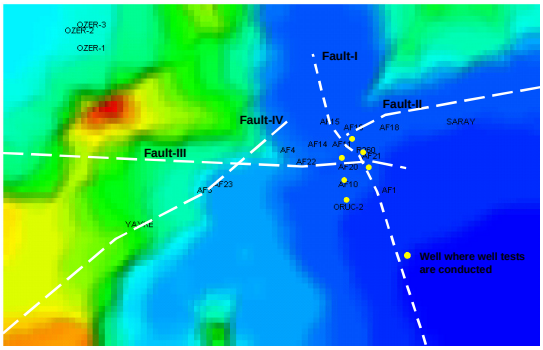

Figure 8. A schematic view showing the wells where well tests are conducted, and possible faults (white dashed lines) in the field.

Unfortunately, we do not have the analytical models in our catalogue to account for all these flow regimes together. Therefore, we considered a rather simpler model based on a partially-penetrating well producing (with changing wellbore-storage and rate-dependent skin effects) between two no-flow parallel faults at least to honor the 1/2 slope line observed after one hour on the deconvolved derivative response (Fig. 6). Fig. 9 presents the match of the unit-rate derivative response derived from deconvolution of the buildup pressures. Fig. 10 presents a comparison of the pressure data generated from this model with the test pressure data during the whole test sequence. (The results shown in Figs. 9 and 10 are based on measured rates and the estimated initial pressure of 280.081 psi.) The model cannot reproduce the measured pressures for the flowing periods, even though we included rate-dependent skin effects (Fig. 10). As discussed previously, this discrepancy may be due to errors in measured flow rates; though we do not know how to correct them or know if the estimated (or adjusted) rates by deconvolution are correct. However, the model reproduces the constant unit-rate drawdown buildup responses derived from deconvolution of buildup pressures (Fig. 9), but it does not, however, reproduce the estimated derivative responses well at early times in the time interval from 0.03 to 0.5 hr. We believe that this is because the model we used cannot incorporate a finite-conductivity fault nearby the well. We note that we obtain a much better match for the early-time portions of the derivative responses by using the model based on a finite-conductivity fault (for a fully penetrating well with changing wellbore-storage effects) given by Abbaszadeh and Cinco-Ley (1995) as shown in Fig. 11. The model fails, however, to reproduce the late-time portions of the buildup after 1 hr, as expected, because it assumes that the zones on both sides of the fault plane are of infinite extent. To match both the early- and late-time portions of the buildup responses we need a finite-conductivity fault model that considers one of the zones as bounded by two parallel no-flow boundaries. The permeability-thickness product (~ 295[1] – 957 Darcy-m), mechanical skin (~ -1.0[1] – -2.5), and distances to the finite conductivity fault (~30[1] m) and no-flow faults (~ 340 m) estimated from both models were reasonable and seems to be consistent with the available geologic model (Fig. 8) and estimated parameters from the tests conducted in other

[1] Estimated values based on the finite-conductivity fault model of Abbaszadeh and Cinco-Ley (1995).

nearby wells. Finally, we should note that we also performed history matches of the test data by using the same models, but with the estimated rates from deconvolution (Fig. 7). The results were similar to those obtained by using measured rates. For example, with the model used to generate the results given in Figs. 9 and 10, we obtained the permeability-thickness product as 1175 Darcy-m, mechanical skin as -2.3, and the distances to the no-flow faults as 330 m. The model match for deconvolved constant rate responses was similar in quality to that shown in Figs. 9 and 11, but the model match for the pressures during the flow periods was much better than that shown in Fig. 10 based on measured rates.

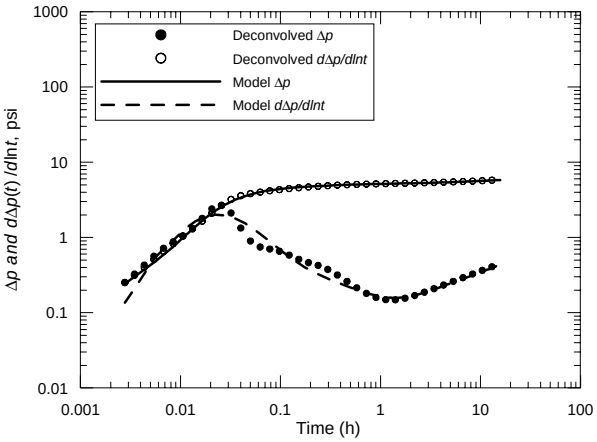

Figure 9. Model match of deconvolved constant rate drawdown responses; the model is a partially penetrating well in a reservoir with two parallel no-flow faults.

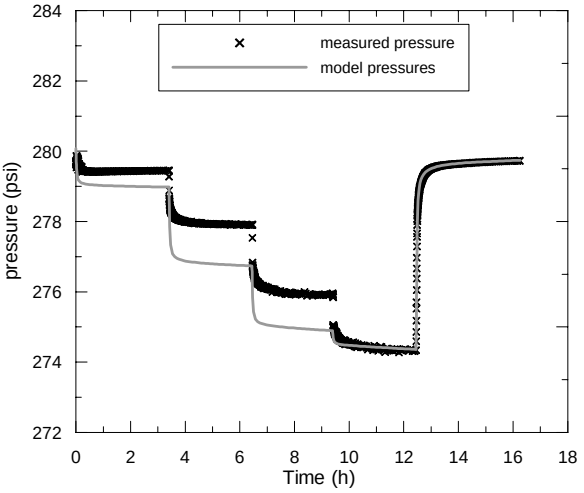

Figure 10. Model match of measured pressure history; the model is a partially penetrating well in a reservoir with two parallel no-flow faults.

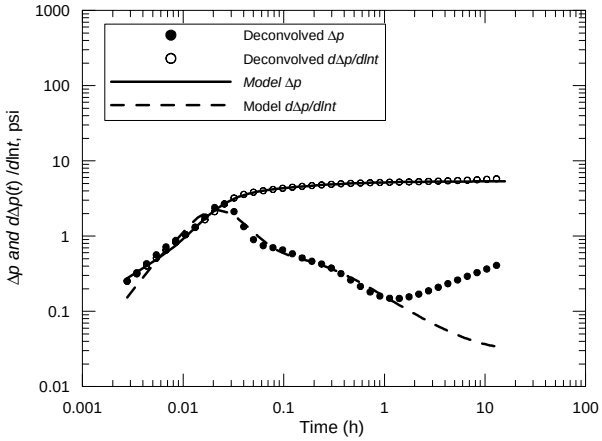

Figure 11. Model match of deconvolved constant rate drawdown responses; the model is a finite conductivity fault model of Abbaszadeh and Cinco-Ley (1995).

The permeability-thickness (*kh*), mechanical skin (*S*), and non-Darcy coefficient (*D*) values estimated from multirate tests conducted at the wells AF-11, AF-16, AF-20, and AF-21 are summarized in Table 3.

Table 2. kh, S, and D values estimated from multirate tests conducted at the wells AF-11, AF-16, AF-20, and AF-21.

Well Name	*kh* (darcy-m)	*S* dimensionless	*D* $(lt/s)^{-1}$
AF-11	201	-3.3	$8.26x10^{-2}$
AF-16	665	-1.1	$1.92x10^{-1}$
AF-20	1085	-4.3	$4.32x10^{-1}$
AF-21	295	-1.0	$6.5x10^{-3}$

3. DRAWDOWN/BUILDUP TESTS

Here, we summarize the results obtained from the analyses of conventional drawdown/buildup tests conducted at the wells R-260, AF-11, AF-16, AF-20, and AF-21. A schematic view of the tested well locations together with the other wells in the field, with possible faults given by the geological model, is shown in Figure 8. The red colors in Fig. 8 show the highest elevations (above sea level), whereas dark blue colors show the lowest elevations.

The drawdown/buildup tests are designed to determine *kh*, skin factor, as well as reservoir characteristics and boundaries if possible. Only the drawdown/buildup test of the well R-260 and its analysis will be presented in detail here.

Figure 12 presents the pressure/rate recorded during the drawdown/buildup test at the well R-260. The pressure data were measured at a depth of 115 m with a down-hole quartz gauge. The temperature of the fluid recorded at this depth is around 103.6 ^{o}C. The total depth of the well is 166 m. The open interval is from 100 m to 166 m, with 8 and 1/2 inches wellbore diameter. As shown in Fig. 12, the first drawdown

period is nearly ten hours at constant production rate of 33.7 lt/s. The duration of the following pressure buildup (PBU) period is 6 hours. After the PBU period, there is another 4-hour flow period with the same flow rate of the first flow period. The total test duration is about 20 hours.

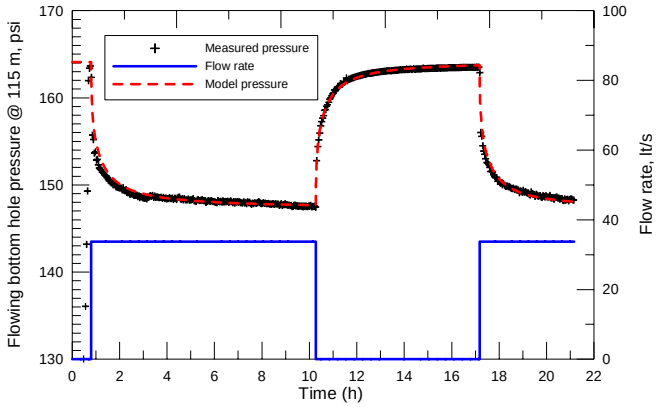

Figure 12. Pressure and rate data for the drawdown/buildup test conducted at the well R-260 (dashed curve represent history-matched model pressure).

The deconvolved constant-rate drawdown pressure and derivative responses (using buildup pressures alone, the flow rate history shown in Fig. 12 and the initial pressure value of 164 psi) obtained from our deconvolution algorithm are shown in Fig. 13. The deconvolution results are compared to the conventional pressure buildup derivatives based on the conventional (radial flow) Agarwal's superposition time (Agarwal, 1980) plotted versus shut-in time. The upward trend observed in conventional buildup-derivative data (blue data points in Fig. 13) near the end of buildup period is due to the right-hand side smoothing effect associated by using Bourdet *et al.* (1989) smoothing method (with a smoothing parameter $L = 0.75$). Hence, this upward trend should not be attributed to the reservoir boundary effects. Deconvolved unit-rate responses (red curves in Fig. 13) provide a 14-hour longer data set than conventional rate- buildup responses and identify a well-defined -1 slope line for almost one-and-a-half log-cycle near the end of the data, indicating an infinite conductivity (or constant-pressure) fault near the well.

The flow regimes indicated by deconvolved constant-rate drawdown derivative data in the time interval from 0.0003 to 1 h are not very conclusive. The deconvolved constant-rate derivative indicate changing wellbore storage or double porosity behavior in the time period from 0.0003 to 0.01 h, and an intersecting fault (one with no-flow, and other is constant-pressure) for times greater than 0.01 h. Another plausible model is a finite-conductivity fault intersecting the well nearby a constant-pressure fault.

Three different plausible models were considered to match the full pressure history shown in Fig. 12. Model 1 refers to a model with two intersecting faults with a right angle (one is a no-flow, and the other is a constant-pressure). Model 2 refers to a model with a single constant-pressure fault, whereas Model 3 refers to a model with a finite-conductivity fracture intersecting the well located near a single-constant pressure fault. The "best" match (based on rms values obtained for the matches, and confidence intervals for parameters) was obtained with Model 1 as shown with a dashed curve in Fig. 12, which also shows the model match (based on Model 1) of the measured pressure data recorded for the entire test sequence. The estimated model parameters are summarized in Table 3. As can be seen from Fig. 12, we have almost a perfect match of measured pressure. A highly negative skin factor (Table 3) gives an indication of a highly permeable fracture/fault network intersecting the well.

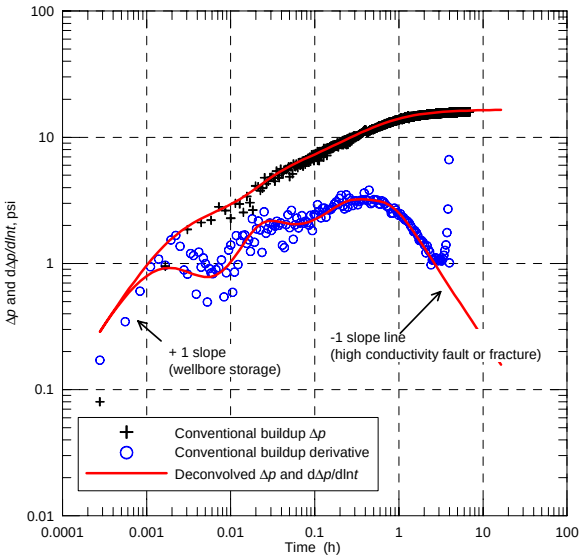

Figure 13. Comparison of deconvolved constant-rate responses derived from buildup pressures with the conventional pressure buildup pressure change and its Bourdet derivative (based on the last rate prior to buildup) for the well R-260.

Table 3. Some input and estimated model parameters for obtaining model match shown in Figure 12.

Model Parameters	
kh (darcy-m)	47.8
p_i, psi	164.09
S (skin, dimensionless)	-4.9
d_{f1}, m (distance to no-flow fault)	63
d_{f2}, m (distance to constant-pressure fault)	126
h, m (formation thickness)	65
μ , cp@103.6 ^{o}C	0.281
r_w, m	0.108
$\phi c_t h$ (m/psi)	2.35×10^{-4}

The kh and skin factor values estimated from drawdown/buildup tests conducted at the well R-260, AF-11, AF-16, AF-20, and AF-21 are summarized in Table 4. Note that the skin factor values given in Table 4 represents total skin (i.e, $s_t = s + Dq$), including both mechanical skin (s) and non-Darcy skin (Dq). As is known (see, for

example, Bourdet, 2002), a constant-rate drawdown/buildup test does not allow one to obtain individual values of mechanical skin and non-Darcy skin (or non-Darcy coefficient, *D*).

Table 4. Permeability-thickness (kh) and total skin values estimated from analyses of drawdown/buildup tests conducted at wells R-260, AF-11,and AF-16.

Well Name	*kh* (darcy-m)	*Total skin* dimensionless
R-260	48	-4.9
AF-11	201	1.96
AF-16	665	10.6

4. INTERFERENCE TESTS

Here, we summarize the results obtained from analyses of two-well interference tests conducted at some of the wells in the field. The well pairs where the interference tests are conducted are AF-21/R-260, AF-21/AF-11, AF-20/AF-10, and AF-20/AF-11. A well name given before the slash indicates an active well, while a well name given after the slash indicates an observation well during the two-well interference test. Here, we only present our analysis for the interference test involved between the wells AF-21 and R-260 in detail. In this test, AF-21 is the active well, while the well R-260 is the observation well. The distance between the two wells is 78.5 m.

Figure 14 presents flow-rate history at the active well (AF-21) and pressure recorded at the observation well (R-260). The bottom-hole pressure at the well R-260 was recorded at a depth of 116 m by a down-hole quartz gauge.

Although it may not be evident from Fig. 14, the production at AF-21 is felt at R-260 in 100 seconds, indicating a highly permeable fracture/fault network existing between the wells. The total test duration after production started at well AF-21 is about 170 h (or about 7 days). The static pressure measured at the well R-260 at the depth of 116 m is 158.5 psi. After first 140 hours of production at AF-21, the well R-260 was shut-in about 6 hours due to some operational problems occurred at the well AF-21. This shut-in period provided a 6-hour buildup test data in the time interval from 182 to 188 h (in cumulative time) as shown Fig. 14.

In Figure 15, we present the deconvolved constant-rate drawdown responses (pressure drop and derivative functions) derived from the buildup pressures alone, and compare these results with the conventional normalized buildup pressure- change and its derivative with respect to Agarwal's equivalent time plotted versus elapsed time. We assume that the initial pressure value of 158.5 psi measured and flow rate history measured prior to buildup (see Fig. 14) are accurate and can be treated as known in deconvolution procedure of Eq. 2.

As can be seen from Fig. 15, deconvolution provides about a one-and-a-half cycle longer data than conventional buildup data and the late portions of deconvolved responses give an indication of a highly finite-conductivity fault near the well.

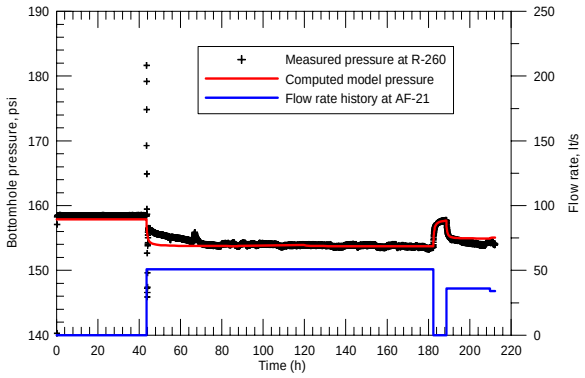

Figure 14 Pressure and flow rate history for the AF-21/R-260 two-well interference test.

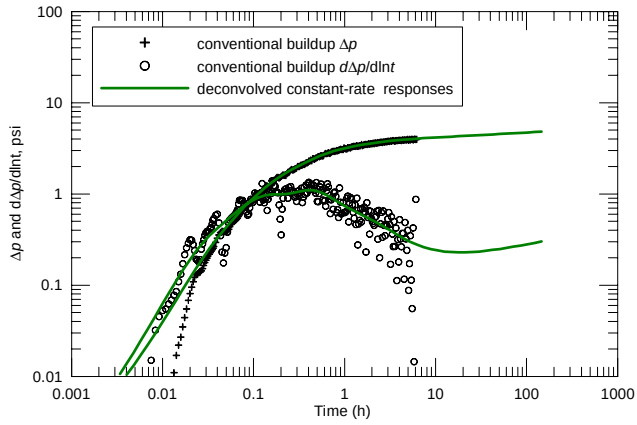

Figure 15. Comparison of deconvolved responses derived from buildup pressures with conventional pressure buildup pressure change and its Bourdet derivative (based on the last rate prior to buildup).

Next, we performed parameter estimation for determining permeability-thickness product (kh) and porosity-compressibility-thickness product ($\phi c_t h$), and the distance (r_i) between the observation well R-260 and an imaginary well by using a "simple" well/reservoir model considering a fully-penetrating well near a constant-pressure fault in a homogeneous isotropic reservoir as we do not have an excess to an analytical solution for an interference well near a finite conductivity fault. The model match of the measured pressure data recorded for the entire interference test sequence is shown in Fig. 14, and the match can be considered as acceptable.

The estimated model parameters are summarized in Table 6. It is important to note that r_i given in Table 5 represents the distance between the well R-260 and an imaginary well, perpendicular to the fault. As is known from the work of Vela (1977), one cannot determine uniquely the distance to the fault and its orientation from a single-interference test. Note also that *kh* value estimated from this interference test is different from *kh* values estimated from the tests where AF-21 and R-260 were pulsing wells alone (see Tables 2 and 4). These results as well as the results given in Table 6 indicate that the geothermal reservoir under consideration is highly heterogeneous and permeable. In addition,

interference tests give an indication that permeability is more developed in the NS direction than in the EW direction.

Table 5. Some input and estimated model parameters for obtaining model match shown in Figure 14.

Model Parameters	
kh (darcy-m)	135
p_i, psi	158.49
r_i, m (distance between the well R-260 and an imaginary well)	382
h, m (formation thickness)	65
μ , *cp*@103.6 ^{o}C	0.281
r_w, m	0.108
$\phi c_t h$ (m/psi)	2.91×10^{-4}

The permeability-thickness (*kh*) and the porosity-compressibility-thickness ($\phi c_t h$) products estimated from all interference tests conducted in the field are summarized in Table 6.

Table6. kh and $\phi c_t h$ values estimated from two—well interference test conducted in the field.

Well Pairs Active/observation	*kh* (darcy-m)	$\phi c_t h$ (m/psi)
AF-21/R-260	135	2.91×10^{-4}
AF-21/AF-11	610	2.98×10^{-3}
AF-20/AF-10	1900	1.06×10^{-2}
AF-20/AF-11	415	2.00×10^{-3}

5. CONCLUSIONS

In this work, we presented analyses of various types of pressure transient tests (such as multirate tests, conventional drawdown and buildup tests, and interference tests) conducted in the Afyon Ömer-Gecek geothermal field, Turkey. In general, the pressure tests analyzed indicate that the wells' productivities are quite high, but influenced by non-Darcy flow effects and are producing in a complex fractured/faulted network system. The estimated values of permeability-thickness products (*kh*) from multirate, drawdown/buildup and interference tests range from 40 to 2000 Darcy-m. The well test data also identify highly conductive (recharging) faults, where we believe these faults are dominating the performance of the geothermal field. Regarding determining these faults orientations in the field, additional pressure transient tests and more detailed geological and geophysical work are recommended.

Deconvolution analysis based on recently proposed robust algorithms by von Schroeter *et al.* (2004), Levitan (2005) and Onur *et al.* (2008) was found useful to extract more information from the well tests conducted in the field.

ACKNOWLEDGEMENTS

We thank the management of AFJET A.Ş. for giving us the permission to use the pressure data presented in this study. The pressure tests were conducted by Iller Bank of Turkey. Some portions of the material presented here were taken from Onur *et al.* (2007).

REFERENCES

Abbaszadeh, M. and Cinco-Ley, H.: Pressure Transient Behavior in a Reservoir With a Finite-Conductivity Fault, *SPE Formation Evaluation* (March 1995) 26.

Agarwal, R.G.: A New Method to Account for Production Time Effects When Drawdown Type Curves Are Used to Analyze Buildup and Other Test Data, paper SPE 9289 presented at the 1980 SPE Annual Technical Conference and Exhibition, Dallas, TX, 21-24 September (1980).

Bourdet, D.: *Well Test Analysis: The Use of Advanced Interpretation Models*, Elsevier, Amsterdam, the Netherlands, 426 pp (2002).

Bourdet, D., Ayoub, J.A., and Pirard, Y.M.: Use of Pressure Derivative in Well-Test Interpretation, *SPE Formation Evaluation* (June 1989) 69.

Levitan, M.M.: Practical Application of Pressure/Rate Deconvolution to Analysis of Real Well Tests, *SPE Reservoir Evaluation and Engineering* (April 2005) 113.

Levitan, M.M., Crawford, G.E., and Hardwick, A.: Practical Considerations for Pressure-Rate Deconvolution of Well-Test Data, *SPE Journal* (March 2006) 35.

Onur, M., Cinar, M., Ilk, D., Valko, P. P., Blasingame, T., Hegeman, P.S.: An Investigation of Recent Deconvolution Methods for Well-Test Data Analysis, Proceedings, *SPE Journal* (June 2008), 226.

Onur, M., Cinar, M., Aksoy, N., Serpen, U., Satman, A.: A Analysis of Well Tests in Afyon Ömer-Gecek Geothermal Field, Turkey, Proceedings, *Thirty-Second Workshop on Geothermal Reservoir Engineering*, Stanford University, Stanford, California, Jan. 22-24 (2007).

Satman, A., Onur, M., Serpen, U, Aksoy, N.: A Study on the Production and Reservoir Performance of Omer-Gecek/Afyon Geothermal Field, Proceedings, *Thirty-Second Workshop on Geothermal Reservoir Engineering*, Stanford University, Stanford, California, Jan. 22-24 (2007).

Vela, S. (), "Effect of a Linear Boundary on Interference and Pulse Tests-The Elliptical Influence Area," Journal of Petroleum Technology (August 1997), 947.

von Schroeter, T., Hollaender, F., and Gringarten, A.C.: Deconvolution of Well Test Data as a Nonlinear Total Least Squares Problem, *SPE Journal* (December 2004) 375.